Effect of dealumination on the catalytic performance of Cr-containing Beta zeolite in carbon dioxide assisted propane dehydrogenation

Piotr Michorczyk, Kamila Zeńczak-Tomera, Barbara Michorczyk, Adam Węgrzyniak, Marcelina Basta, Yannick Millot, Laetitia Valentin, Stanislaw Dzwigaj

Contents lists available at ScienceDirect

Journal of CO2 Utilization

journal homepage: www.elsevier.com

Effect of dealumination on the catalytic performance of Cr-containing Beta zeolite in carbon dioxide assisted propane dehydrogenation

Piotr Michorczyk [a,*], Kamila Zeńczak-Tomera [a], Barbara Michorczyk [a], Adam Węgrzyniak [a], Marcelina Basta [a], Yannick Millot [b], Laetitia Valentin [b], Stanislaw Dzwigaj [b,*]

[a] Institute of Organic Chemistry and Technology, Cracow University of Technology, Warszawska 24, 31-155 Kraków, Poland
[b] Laboratoire de Réactivité de Surface, Sorbonne Université-CNRS, UMR 7197, 4 place Jussieu, Case 168, F-75252 Paris, France

ARTICLE INFO

Keywords:
Propene
Dehydrogenation
Utilization of CO_2
Beta zeolite
Chromium oxide-based catalyst

ABSTRACT

New active and selective catalysts for propane to propene dehydrogenation in assistance of CO_2 (CO_2-PDH) were prepared by chromium incorporation in siliceous SiBeta. The Cr-containing SiBeta zeolite catalysts were obtained by two-step postsynthesis preparation procedure which consist, in the first step, removal of aluminum from TEABeta zeolite with Si/Al of 17 by treatment with nitric acid solution to obtain an aluminium-free Si-Beta support with Si/Al ratio of 1000 and, in the second step, various amounts of Cr were introduced into the siliceous SiBeta zeolite structure by wet impregnation. The well correlation between the number of redox Cr sites and propene yield up to 2 wt % of Cr has been determined. Comparing of catalytic activity of Cr-containing Beta zeolite catalysts with the identical Cr content (2 wt % of Cr) supported on SiBeta and AlBeta revealed that the dealumination has great impact on catalytic properties. Low acidity of SiBeta is suitable for achieving high selectivity to propene (above 80 %) while high acidity of starting AlBeta promotes propane cracking to lighter hydrocarbons. Moreover, in switch operation mode between propane dehydrogenation in presence and absence of CO_2 the formation rate of propene raises in mode with CO_2 only over Cr-containing SiBeta zeolite catalyst, while over Cr-containing AlBeta zeolite catalyst a negative effect on the rate of propene formation was observed.

1. Introduction

Nowadays unsaturated hydrocarbons are basic and most important intermediates for chemical industry. Particularly, the demand for propene has been growing since it has found an assured position on the chemical raw material and monomers market due to its numerous uses. Worldwide demand for propene currently reaches 90 million tonnes per year and at an estimated growth rate of about 5 % annually, will reach a value of around 130 million tonnes by 2023 [1]. It is estimated that such high demand for propene won't be satisfied by its current two most important sources, that is, steam cracking and catalytic cracking, in which propene is obtained as co-products. Attempts at increasing propene production, e.g. through optimisation of conditions of these processes, will negatively influence the production of other important co-products. Thus, selective processes dedicated solely to propene synthesis, such as propane dehydrogenation, olefin metathesis, and propene synthesis using methanol (e.g. MTP - methanol-to-propene), will gain significance with time.

Concerns connected to meeting demand for propene without simultaneously decreasing production of remaining valuable products also favour intensification of fundamental research. One of the crucial research directions is the development of a new selective process of obtaining propene from propane that could replace propane dehydrogenation process (PDH) currently used for industrial needs. However, this process has disadvantages such as reversibility and endothermalness. An attractive alternative for the traditional PDH is propane oxidative dehydrogenation in the presence of O_2 (ODH) or propane dehydrogenation in the presence of CO_2 (CO_2-PDH). A shared characteristic of all the aforementioned processes is utilising a co-reagent that either removes PDH thermodynamic limits or increases production through hydrogen binding in consecutive reactions. Typically in this process per-

* Corresponding authors.
Email addresses: pmichor@pk.edu.pl (P. Michorczyk); stanislaw.dzwigaj@upmc.fr (S. Dzwigaj)

https://doi.org/10.1016/j.jcou.2019.09.018
Received 23 July 2019; Received in revised form 12 September 2019; Accepted 25 September 2019
Available online xxx
2212-9820/

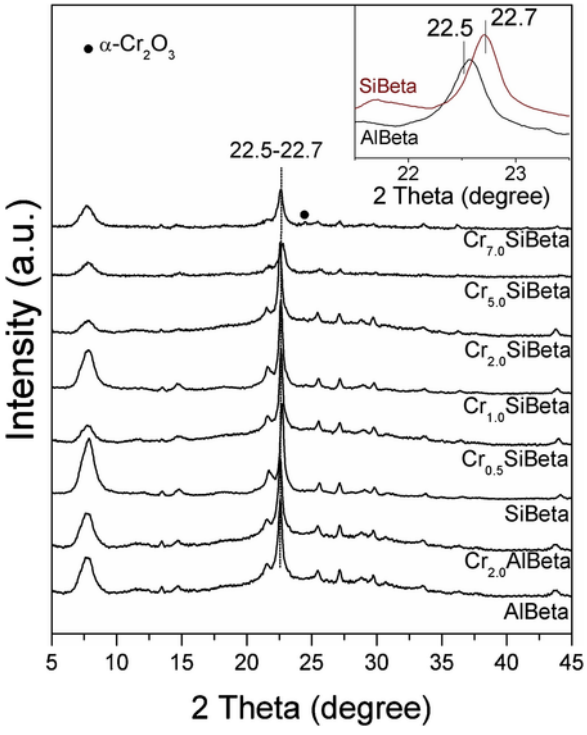

Fig. 1. XRD of AlBeta, SiBeta, $Cr_{0.5}$SiBeta, $Cr_{1.0}$SiBeta, $Cr_{2.0}$SiBeta, $Cr_{5.0}$SiBeta and $Cr_{7.0}$SiBeta recorded at room temperature and ambient atmosphere.

pass conversion of propane and yield of propene are higher than in commercial non-oxidative dehydrogenation. Moreover, due to large scale propene production the process can be attractive way for chemical CO_2 utilisation, because in addition to propene, hydrogen and carbon monoxide (syngas) are produced as the main products. Some possibility of CO_2-PDH integration with syngas or propene required processes are proposed previously [2].

Many different catalysts were investigated in CO_2-PDH containing Pt [3], Ni-Fe [4] Cr [5–16], Ga [17–20], In-Al [21–23], Fe [24] or V [25,26]. Among them, the chromium oxide-based materials are considered as a very promising for CO_2-PDH due to high activity and selectivity. The mechanism of propane dehydrogenation in presence of CO_2 is complex. Various possible scenarios of the CO_2-PDH in which propene is produced either by non-oxidative dehydrogenation with participation of Cr(II) or/and Cr(III) species or by various redox mechanisms with participation of carbon dioxide as a mild oxidant in an oxidative dehydrogenation pathway have been proposed [10,27–31]. In the oxidative pathway various redox cycles between the oxidised/reduced forms of Cr sites, such as Cr(III)/Cr(II), Cr(VI)/Cr(III) or Cr(V)/Cr(III) has been suggested. It has been recognized that high dispersion and presence of redox chromium species are important factors for achieving high catalytic performance in CO_2-PDH [18,27,28]. From above reasons chromium is typically dispersed on a support. Very good support ensuring high chromium dispersion is silica, particularly of ordered mesoporous structure. Due to large specific surface area (in the most cases above 1000 $m^2 g^{-1}$) of mesoporous materials like MCM-41, SBA-1, SBA-15 or MSU_x a high dispersion and concentration of chromium oxide species can be obtained in comparison to unordered silica support [6,9,10,14,18,27,28]. Others tested support, for instance γ-Al_2O_3, which is commercially used for chromium dispersion in PDH catalyst (CATOFIN Process) or active carbon are less useful. Over γ-Al_2O_3 supported chromium oxide catalysts CO_2 addition exerts poisoning effect while in the case of active carbon supported catalyst an application in CO_2-PDH is limited by period regeneration with air [5,11,32].

In this work Cr-containing Beta zeolites were investigated as a catalysts for propane dehydrogenation in the presence of carbon dioxide. Beta zeolite was applied due to a three-dimensional structure, the pores larger than those of ZSM-5 with 12-membered ring openings (0.75 by 0.57 nm for linear and 0.65 by 0.56 nm for tortuous channels), a high thermal and acid stability and a large specific surface area needed for high chromium species dispersion [33–35]. We have shown that dealumination of Beta and subsequently chromium dispersion by simple impregnation procedure give excellent catalysts for CO_2-PDH.

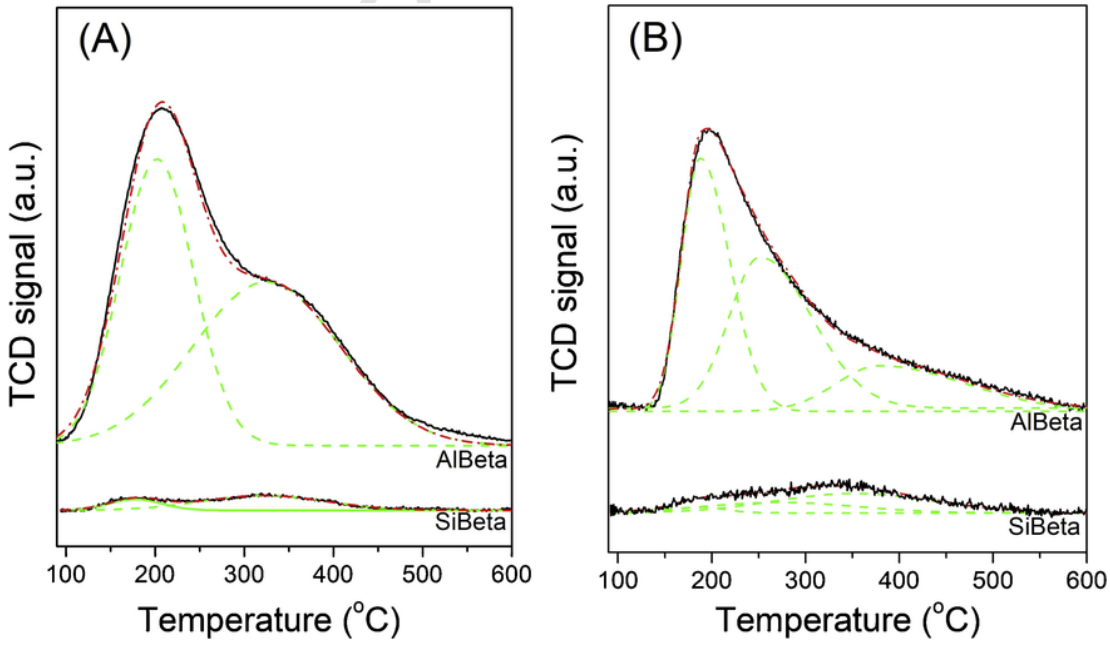

Fig. 2. Thermodesorption profiles of ammonia (A) and carbon dioxide (B) for AlBeta and SiBeta.

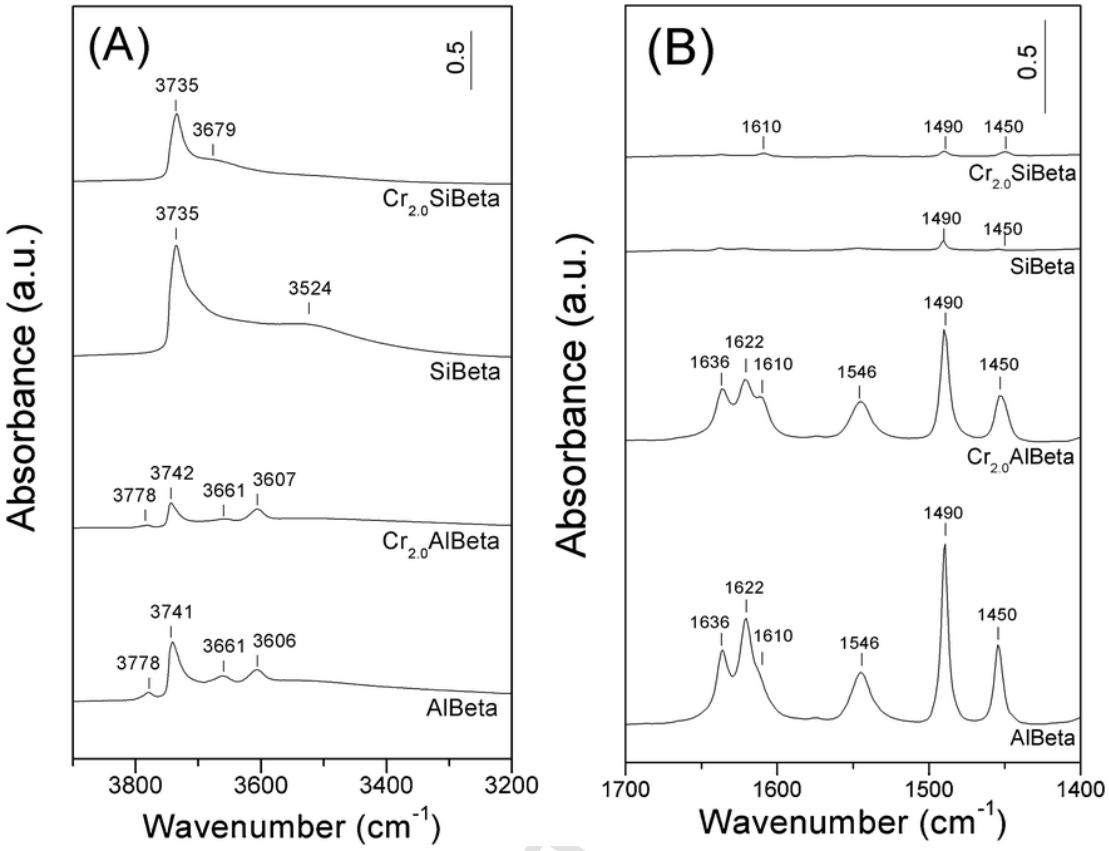

Fig. 3. FTIR spectra recorded at room temperature of AlBeta, $Cr_{2.0}$AlBeta, SiBeta and $Cr_{2.0}$SiBeta for activated (calcined at 723 K for 3 h in O_2 (1.6 10^4 Pa) and then outgassed at 573 K (10^{-3} Pa) for 1 h) (Fig. 3A) and after adsorption of pyridine (133 Pa) for 1 h at room temperature and desorption at 423 K for 1 (Fig. 3B).

Table 1
Acid-base properties of AlBeta and SiBeta determined by NH_3-TPD, pyridine adsorption and CO_2-TPD.

Sample	Acidity					Basicity		
	NH_3-TPD (mmol NH_3 ·g^{-1})			Pyridine adsorption and desorption at 150 °C - FTIR		CO_2-TPD (mmol CO_2 g^{-1})		
	LT	HT	Total	PyH^+ 1545 cm^{-1} [μmol g^{-1}]	PyL 1445–1455 cm^{-1} [μmol g^{-1}]	LT	HT	Total
SiBeta	0.01	0.04	0.06	12	10	0.01	0.01	0.02
AlBeta	0.60	0.69	1.29	235.6	134.9	0.13	0.03	0.16

2. Experimental

2.1. Materials preparation

The AlBeta support with a Si/Al atomic ratio of 17 was obtained by calcination of tetraethylammonium Beta (TEABeta) parent zeolite in air at 550 °C for 15 h. The SiBeta support with a Si/Al atomic ratio of 1000 was obtained by a treatment of TEABeta with 13 mol L^{-1} HNO_3 solution at 80 °C for 4 h, washed with distilled water and dried at 95 °C overnight.

Chromium-containing SiBeta catalysts were obtained by two-step postsynthesis methodwet impregnation. In typical procedure, the SiBeta was contacted with an aqueous chromium nitrate solutions containing from 0.8 to 15.2·10^{-3} mol L^{-1} $Cr(NO_3)_3$·$9H_2O$ and AlBeta was contacted with solution containing 3.2·10^{-3} mol L^{-1} $Cr(NO_3)_3$·$9H_2O$. Then, the separation of the solids from the suspensions were done in evaporator under vacuum of a membrane pump for 2 h in air at 60 °C. Finally, all materials were calcined at 550 °C for 6 h. The sample with SiBeta contained 0.5, 1, 2, 5 and 7 wt % of Cr were labelled as $Cr_{0.5}$SiBeta, $Cr_{1.0}$SiBeta, $Cr_{2.0}$SiBeta, $Cr_{5.0}$SiBeta and $Cr_{7.0}$SiBeta and this with AlBeta, containing 2 wt % of Cr was labelled as $Cr_{2.0}$AlBeta.

2.2. Materials characterization

Textural properties of supports and catalysts were determined from the low-temperature adsorption/desorption isotherms using the Micromeritics (ASAP 2020). Priori to measurements the samples were degassed under vacuum at 350 °C for 12 h. Total pore volume were measured for the value of $p/p_0 = 0{,}98$ and the surface area of the samples were calculated from nitrogen isotherm data using BET and Langmuir models. The micropore volume was determined using the t-plot method.

Powder X-ray diffraction (XRD) analysis of supports and catalysts were performed on a Bruker D8 ADVANCE using Cu K_α radiation ($\lambda = 154{,}05$ pm) in 2θ range of 5–45°.

Analysis of the acidic properties of samples was performed by adsorption of pyridine (Py) followed by infrared spectroscopy. Before analysis, the samples were pressed at ~1 ton cm^{-2} into thin wafers of

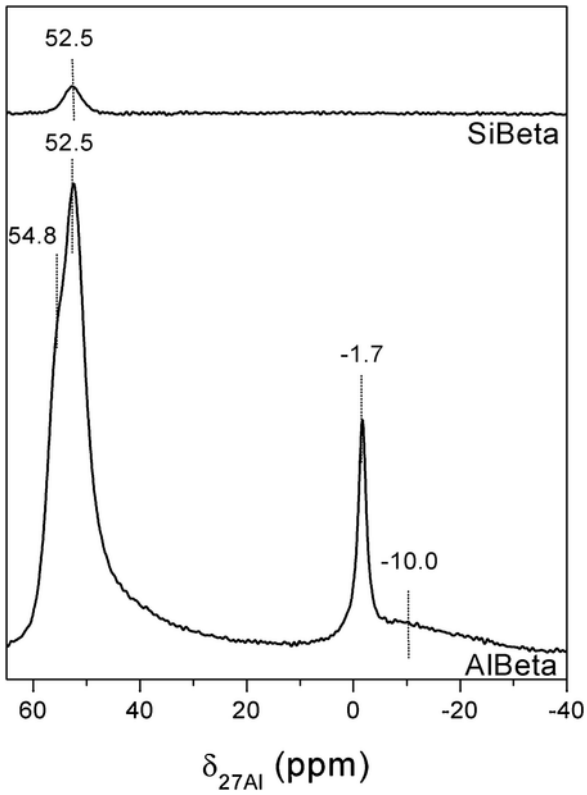

Fig. 4. ^{27}Al MAS NMR recorded at room temperature of AlBeta and SiBeta supports in 4 mm (external diameter) zirconia rotor.

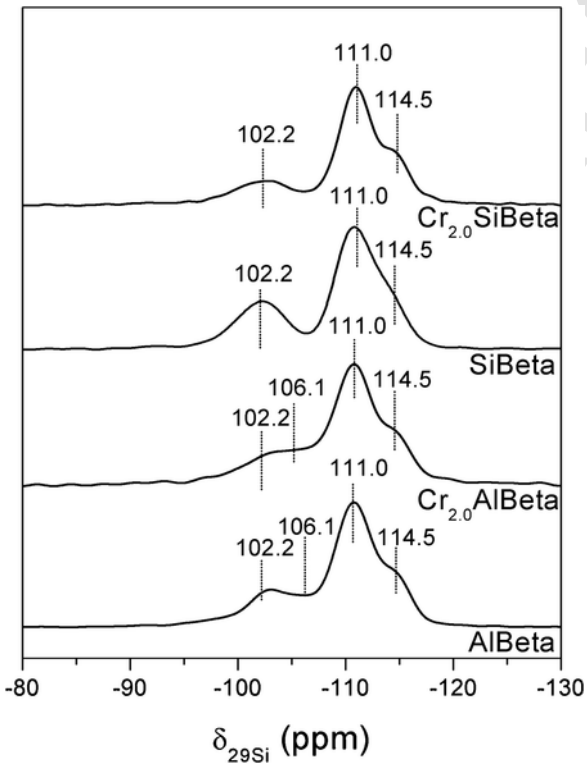

Fig. 5. ^{29}Si MAS NMR recorded at room temperature of AlBeta, $Cr_{2.0}$AlBeta, SiBeta and $Cr_{2.0}$SiBeta.

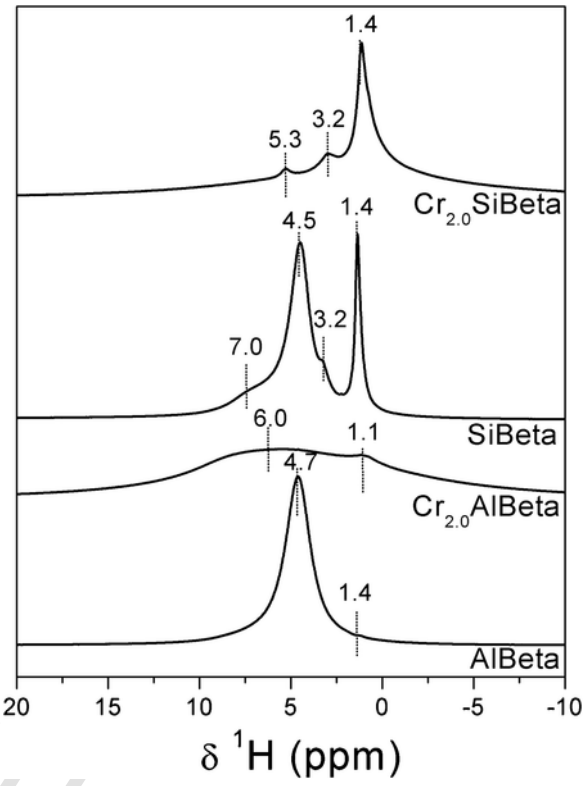

Fig. 6. ^{1}H MAS NMR recorded at room temperature of AlBeta, $Cr_{2.0}$AlBeta, SiBeta and $Cr_{2.0}$SiBeta.

ca. 10 mg cm^{-2} and placed inside the IR cell. Then, the wafers were activated by calcination in static conditions at 723 K for 3 h in O_2 ($1.6 \cdot 10^4$ Pa) andoutgassed at 573 K (10^{-3} Pa) for 1 h. After the wafers were contacted at room temperature with gaseous Py (133 Pa). The IR spectra were recorded after desorption at room temperature and 423 K for 1 h with a Bruker Vector 22 spectrometer (resolution 2 cm^{-1}, 128 scans). The reported spectra were obtained after subtraction of the spectrum recorded before Py adsorption.

^{29}Si MAS NMR spectra were recorded at 99.3 MHz with Bruker AVANCE 500 spectrometer and 7 mm zirconia rotors spinning at 5 kHz. Tetramethylsilane was used as reference. ^{29}Si MAS NMR spectra were recorded with a 4.2 μs excitation pulse and a 10 s recycle delay.

^{27}Al and ^{1}H MAS NMR experiments were performed using a 4 mm zirconia rotors spinning at 12 kHz. The resonance frequency of 500.16 MHz and 130.33 MHz were used for recording of ^{1}H and ^{27}Al, respectively. An aqueous $Al(NO_3)_3$ 1 N solution was used as second reference to determine chemical shifts. ^{1}H MAS NMR was recorded with a 90° pulse duration of 2.9 μs and a recycle delay of 5 s and 16 accumulations. A small-flip-angle technique with a pulse of 1.2 μs (π/8), 0.5 s for the recycle delay and 2048 accumulations was used for recorded ^{27}Al MAS NMR.

The total Cr content (Cr_{ICP}) in the samples was determined using an Optima 2100 DV (Perkin-Elmer, USA) ICP-OES instrument, equipped with axially viewed plasma. In the typical mineralization procedure, a sample (ca. 50 mg) was crashed and mixed with 2 g of $NaNO_3$ (POCh-Polish Chemical Reagents) and 2 g of NaOH (POCh-Polish Chemical Reagents) in a melting pot. Then, the mixture was heated to 600 °C in air. The mineralization mixture was cooled to RT, dissolved in deionized water and filtered. Cr_{ICP} was determined in a dissolved solution.

Temperature-programmed desorption of ammonia (NH_3-TPD) and reduction with hydrogen (H_2-TPR) experiments were carried out using microreactor connected on-line with a GC equipped with a thermal conductivity detector. In NH_3-TPD measurements about 0.1 g sample

Table 2
Cr content, specific surface area, porosity and redox properties of Cr_xSiBeta catalysts.

Sample	Cr_{ICP} content (wt %)	S_{BET} ($m^2 g^{-1}$)	$S_{Langmuir}$ ($m^2 g^{-1}$)	V_{micro} ($cm^3 g^{-1}$)	V_{total} ($cm^3 g^{-1}$)	H_2-TPR	
						H_2 consumption (mmol g_{cat}^{-1})	H_2/Cr_{ICP} (mol/mol)
$Cr_{0.5}$SiBeta	0.55	627	724	0.22	0.42	0.13	1.46
$Cr_{1.0}$SiBeta	1.15	621	713	0.20	0.41	0.23	1.34
$Cr_{2.0}$ SiBeta	2.14	554	644	0.16	0.34	0.42	1.14
$Cr_{5.0}$SiBeta	4.96	552	640	0.19	0.37	0.73	0.84
$Cr_{7.0}$SiBeta	6.40	517	597	0.17	0.35	1.18	0.81
$Cr_{2.0}$AlBeta	2.20	618	713	0.20	0.41	0.46	1.18

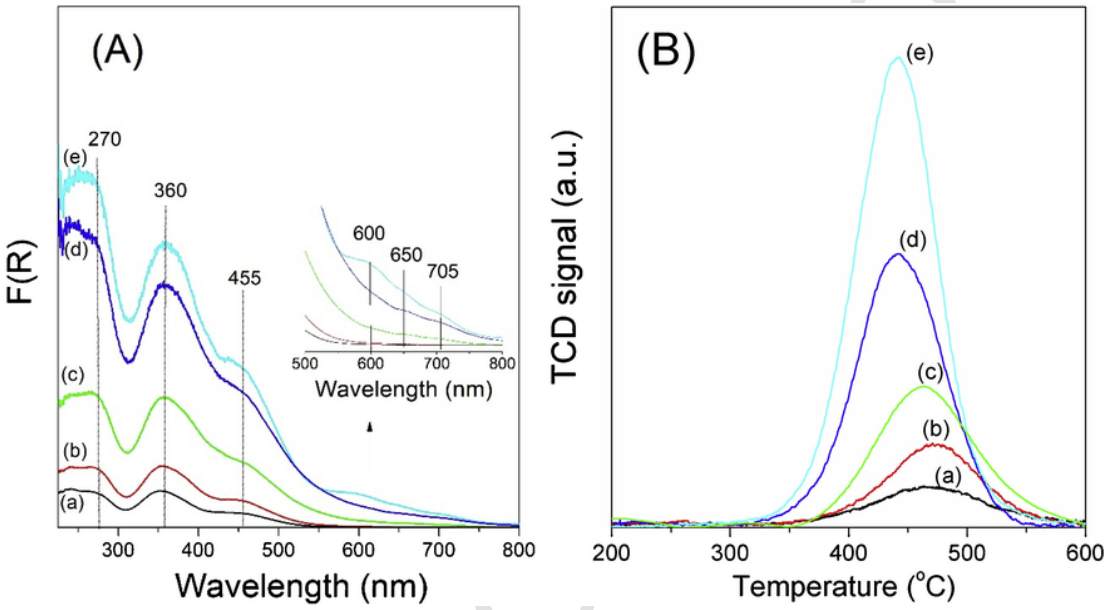

Fig. 7. UV–vis DRS spectra recorded at room temperature and H_2-TPR profiles of (a) $Cr_{0.5}$SiBEA, (b) $Cr_{1.0}$SiBEA, (c) $Cr_{2.0}$SiBEA, (d) $Cr_{5.0}$SiBEA and (e) $Cr_{7.0}$SiBEA zeolite catalysts.

Table 3
Catalytic performance of chromium-containing Beta catalysts and other supported chromium oxide-based catalysts in CO_2-PDH process.

Sample	Reaction temperature	Specific activity × 10^6 (mol s^{-1} g_{cat}^{-1})	Conversion (%)		Yield (%)	Selectivity (%)				References
			C_3H_8	CO_2	C_3H_6	C_3H_6	C_2H_6	C_2H_4	CH_4	
$Cr_{0.5}$SiBeta	550	0.82	11.0	0.6	10.1	94.7	1.5	3.6	2.8	This work[a]
$Cr_{1.0}$SiBeta	550	1.31	17.6	1.2	16.0	90.8	1.4	4.5	3.3	
$Cr_{2.0}$SiBeta	550	1.85	24.8	4.0	21.6	87.1	2.4	4.2	6.2	
$Cr_{5.0}$SiBeta	550	2.05	27.6	5.5	23.3	84.4	2.8	4.0	8.8	
$Cr_{7.0}$SiBeta	550	2.48	33.3	7.0	27.2	81.6	3.7	4.0	10.7	
$Cr_{2.0}$AlBeta	550	0.33	4.5	0.8	2.0	45.1	8.0	25	21.9	
$Cr_{5.0}$/AC[b]	550	n.r.[c]	39.8	n.r.	34.5	86.7	1.6	2.8	7.5	[32]
$Cr_{3.4}$/D[d]	600	n.r.	19.7	n.r.	11.8	59.6	7.3[e]		5.4	[7]
$Cr_{3.4}/Al_2O_3$	550	n.r.	3.3	n.r.	3.3	92.9	0.5	1.6	5.0	[5]
$Cr_{3.4}/SiO_2$	550	1.6	15.4	1.3	14.3	92.6	1.3	2.5	3.6	[28]
$Cr_{5.0}/ZrO_2$	550	n.r.	58	42	30	n.r.				[60]
$Cr_{3.4}$/MCM-41	600	n.r.	39.4	6.7	34.9	88.5	2.9	2.5	6.1	[14]
Cr_x/ZSM-5-S	550	n.r.	48.3	n.r.	41.5	86.0	2.0	4.8	7.2	[61]
$Cr_{3.4}$/SBA-1	550	2.60	33.2	4.6	29.2	87.9	2.9	3.3	5.9	[28]
$Cr_{3.4}$/SBA-15	550	2.20	27.2	3.4	24.3	89.3	2.4	3.5	4.7	[28]
$Cr_{5.0}$/MSUx	600	n.r.	28.0	n.r.	26.6	95.0	n.r.	n.r.	n.r.	[15]

[a] Reaction conditions: C_3H_8:CO_2:He molar ratio = 1:5:9; Total flow rate = 30 $cm^3 min^{-1}$; Catalyst weight = 200 mg; WHSV = 1.2 h^{-1}; Catalytic test results summarized after 10 min.
[b] AC- activated carbon.
[c] n.r.- not reported.
[d] D- diamond.
[e] Sum of ethane and ethene selectivity.

(mixed with SiC to constant volume 1,5 mL) was preheated under helium (99.999 vol %, Linde) with heating rate 10 °C min^{-1} to 550 °C, kept for 2 h, and then cooled to 100 °C under the same atmosphere. Subsequently, ammonia (99.98 vol %, Linde) at flow rate 20 mL min^{-1} for 30 min were adsorbed at 100 °C. The sample was then flashed by helium at a flow rate 30 mL min^{-1} for 2 h. The NH_3-TPD measurement

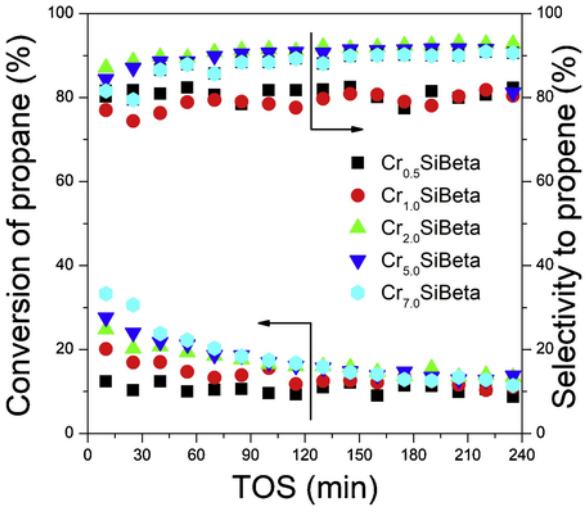

Fig. 8. Conversion of propane and selectivity to propene vs. TOS in CO_2-PDH process over $Cr_xSiBeta$ series. Reaction conditions: T = 550 °C; C_3H_8:CO_2:He molar ratio = 1:5:9; Total flow rate = 30 $cm^3 min^{-1}$; Catalyst weight = 200 mg; WHSV = 1.2 h^{-1}.

was conducted by heating the sample from 100 °C to 800 °C with the heating rate of 10 °C min^{-1}.

In H_2-TPR experiments 0.1 g of sample dilute with SiC was first preheated in air flow for 30 min at 550 °C and then in dry He (99.999 vol. %, Linde,) stream for next 30 min. After that the sample was cooled down in the He stream to 100 °C. The H_2-TPR analysis was then performed using mixture of N_2/H_2 (95/5 vol. %, Air Liquide) environment at a total flow rate 30 mL min^{-1} and ramped from 100 to 650 °C with heating rate of 10 °C min^{-1}. The H_2 consumption was measured using TCD and NiO (99.999 %, Aldrich) was used as a reference for the calibration of H_2 consumption.

Diffuse reflectance UV–vis analysis was conducted using an Ocean Optics HR2000+ spectrometer (integration time 50 ms, 50 scans) equipped with an DH-2000 BAL halogen-deuterium light source. The spectra were recorded between 225 to 800 nm and barium sulfate (99% Sigma-Aldrich) was use as a standard.

During selected catalytic tests carried out at 550 °C experiments with the oxidation state of chromium species was monitored using UV–vis equipment mentioned above (integration time 25 ms, 25 scans) and a high temperature reflection probe (FCR-7UV400-2-ME-HTX, 7 × 400 μm fibers). The probe was attached at the top of quartz microreactor within the distance of 2–3 mm from catalyst bed.

2.3. Catalyst evaluation

CO_2-PDH reaction was carried out in a flow-type quartz reactor. Typically, 0.2 g of the catalyst (grain size 0.2–0.3 mm) was preheated in a stream of dry helium (99.999 vol. %, Linde) for 30 min at 550 °C before each catalytic measurements, and then the reaction was started at 550 °C under atmospheric pressure. The feed consisted of a mixture of propane (99.96 vol %, Linde) and CO_2 (99.996 vol %, Linde) diluted with helium. The volumetric ratio of CO_2/C_3H_8/He = 5/1/9 was introduced into the reactor at a flow rate of 30 mL min^{-1}. In reference catalytic test without CO_2 (non-oxidative dehydrogenation) the volumetric ratio of C_3H_8/ He = 1/14 was used.

The composition of the reactor exhaust was analyzed by gas chromatograph (Agilent 6890 N) which was equipped with a thermal conductivity detector, Hayesep Q and molecular sieve 5A columns. H_2, CO_2, C_2H_4, C_2H_6, C_3H_6 and C_3H_8 were separated by Hayesep Q column

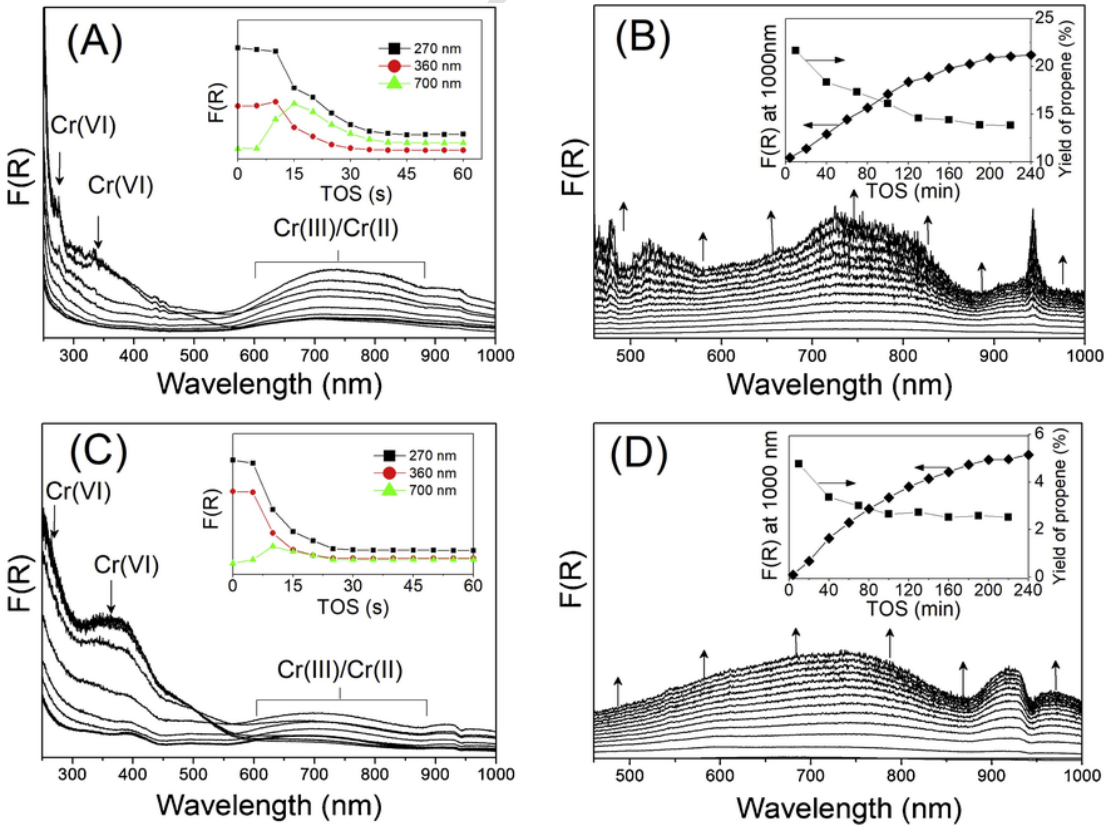

Fig. 9. UV–vis DRS spectra recorded during CO_2-PDH at 550 °C over $Cr_{2.0}$SiBeta (A and B) and $Cr_{2.0}$AlBeta (C and D). Spectra show in region between 0–1 min (A and C) and between 1–240 min (B and D) in interval 5 s. and 10 min, respectively.

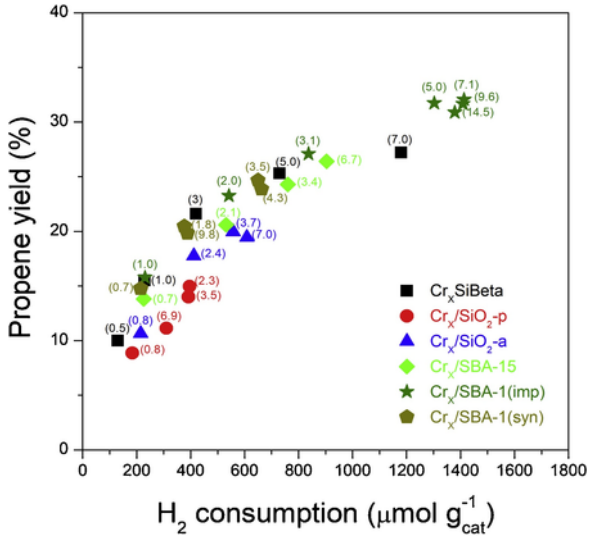

Fig. 10. The variation of propene yield with hydrogen consumption (proportional to number of Cr redox species) for several different chromium oxide based catalysts. Hydrogen consumption was calculated per catalysts weight based on H_2-TPR experiments. Sample notations: Cr_x/SBA-1(imp), Cr_x/SBA-15, Cr_x/SiO_2-a (silica support from Aldrich) and Cr_x/SiO_2-p (silica support from Polish Chemical Reagents) catalysts obtained by impregnation [28]; Cr_x/SBA-1(syn) catalyst prepared by Cr incorporation during SBA-1 synthesis [65]; The values in the brackets indicates total Cr content in the catalysts.

while CH_4 and CO were separated using column with molecular sieve 5A.

Activity normalized per catalyst weight (1), conversion of propane (2) and carbon dioxide (3), yield of propene (4) and selectivity to hydrocarbon products (5) were calculated as:

$$Specific\ activity\ \left(mmol \cdot s^{-1} \cdot g_{cat.}^{-1}\right) = F_{C_3H_8} \cdot C_{C_3H_8} \quad (1)$$

$$Yield\ of\ propene\ (\%) = \frac{n_{C_3H_6,outlet}}{n_{C_3H_8,inlet}} \cdot 100\% \quad (2)$$

$$Conversion\ of\ propane\ (\%) = \frac{n_{C_3H_8,inlet} - n_{C_3H_8,outlet}}{n_{C_3H_8,inlet}} \cdot 100\% \quad (3)$$

$$Conversion\ of\ carbon\ dioxide\ (\%) = \frac{n_{CO_2,inlet} - n_{CO_2,outlet}}{n_{CO_2,inlet}} \cdot 100\% \quad (4)$$

$$Selectivity\ (\%) = \frac{\frac{a_i}{3} \cdot n_i}{n_{C_3H_8,inlet} - n_{C_3H_8,outlet}} \cdot 100\% \quad (5)$$

where: $F_{C3H8,}$ is a number of propane moles per second, C_{C3H8} is conversion of propane per gram of a catalyst $n_{C_3H_8,inlet}$, $n_{CO_2,inlet}$ and $n_{C_3H_8,outlet}$, $n_{CO_2,outlet}$ are numbers of propane and carbon dioxide moles in the reactor inlet and outlet, respectively, $n_{C_3H_6,outlet}$ is a number of propene moles in the reactor outlet, a_i is a number of carbon atoms in a product, and n_i is a number of moles of *"i"* product.

3. Results and discussion

3.1. Support characterization

Initially, AlBeta (Si/Al = 17) and SiBeta (Si/Al = 1000) were characterized for clarify dealumination effect on structure, texture and acid-base properties. As shown in Fig. 1, the crystallinity of Beta zeolite is preserved after dealumination and in the SiBeta support any extra lattice crystalline compounds and long range amorphization do not occur. The increase of 2 theta value of the main diffraction line after dealumination from 22.5 (AlBeta) to 22.7° (SiBeta) indicates contraction of the Beta matrix, in line with earlier investigations (Fig. 1 inset) [36,37].

Moreover, the dealumination leads to small change in porosity and specific surface area. After HNO_3 treatment the BET specific surface area (S_{BET}) increases from 642 m^2 g^{-1} (AlBeta) to 724 m^2 g^{-1} (SiBeta) while the total pore volume from 0.52 $cm^3 g^{-1}$ (AlBeta) to 0.72 cm^3 g^{-1} (SiBeta) [38]. In contrary to structure and texture changes the dea-

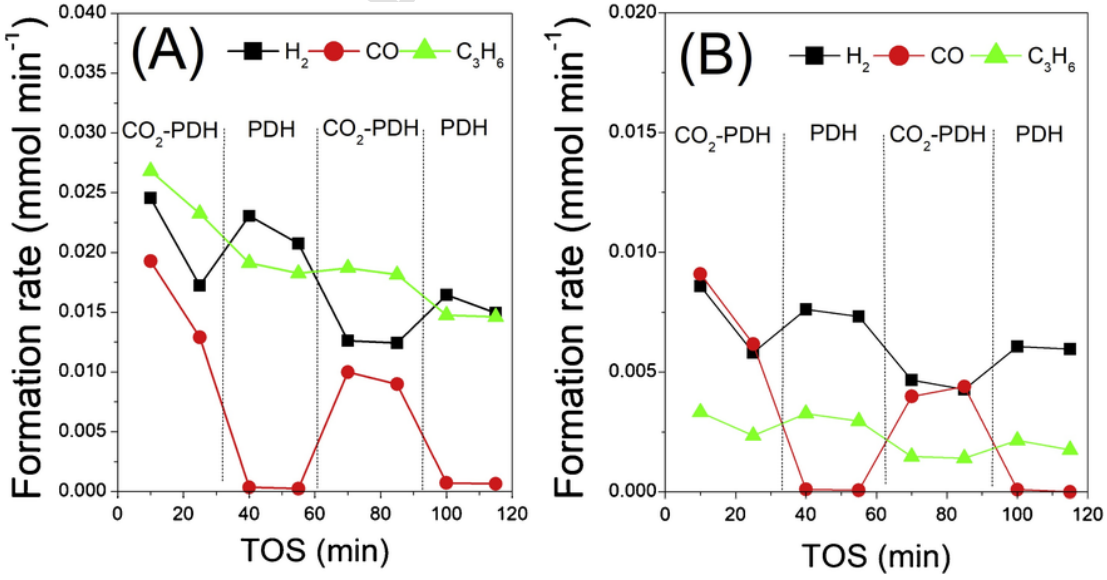

Fig. 11. Rate of propene formation (▲), hydrogen (■) and carbon monoxide (●) in dehydrogenation of propane to propene in the presence (CO_2-PDH) and absence (PDH) of CO_2 at 550 °C over (A) $Cr_{2.0}$SiBeta and (B) $Cr_{2.0}$AlBeta catalysts.

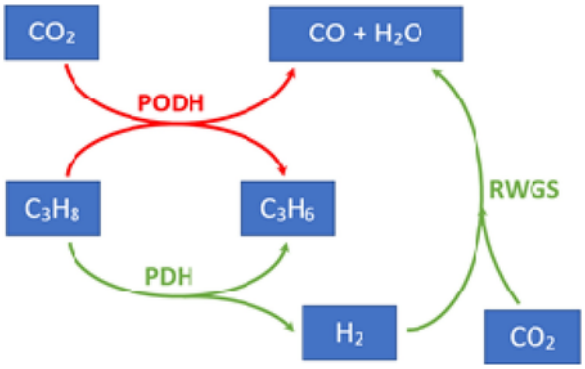

Scheme 1. Possible pathways of propene generation in assistance of CO_2 over Cr-containing SiBeta zeolite catalyst. Red arrows - propane oxidative dehydrogenation (PODH); Green arrows: propane dehydrogenation (PDH) coupling with revers water-gas shift (RWGS).

lumination has much significant impact on acidity. The NH_3-TPD profiles for AlBeta and SiBeta are compared on Fig. 2A. In both cases two maxima at 200 °C and 370 °C are observed on the NH_3-TPD profiles suggesting the presence of two type of acid sites, such as Lewis acid sites related to the presence in zeolite structure of Al^{3+} ions (maximum at around of 200 °C) and Bronsted acid sites related to the acidic proton of Si—O(H) —Al groups (maximum at around of 370 °C), in agreement with earlier reports [39,40].

However, the intensity of these two peaks on SiBeta profile is much lower than on AlBeta profile indicating clearly that dealumination leads to significant reduction of acid sites number.

Presence of both type acidic sites is confirmed by FTIR investigation with pyridine as probe molecule Fig. 3.

The treatment of AlBeta zeolite with HNO_3 solution involve of elimination of Al atoms from the framework evidenced by disappearance of IR bands at 3778, 3661 and 3606 cm^{-1} related to AlO—H groups (Fig. 3A), in agreement with our earlier investigation [41–43]. The appearance of narrow band at 3735 and shoulder at 3710 cm^{-1} related to isolated silanol groups and of a broad band at 3524 cm^{-1} due to H-bonded SiOH groups in SiBeta reveals the presence of vacant T-atom sites [41,44]. As shown in Table 1, the number of Brønsted and Lewis acid sites decrease strongly when AlBeta zeolite is dealuminated and only traces of Brønsted and Lewis acid sites are detected in SiBeta.

To determine the nature and strength of acidic centres in AlBeta, $Cr_{2.0}$AlBeta, SiBeta and $Cr_{2.0}$SiBeta zeolite samples, the adsorption of pyridine as probe molecules has been performed. Fig. 3B presents the FTIR spectra of AlBeta, $Cr_{2.0}$AlBeta, SiBeta and $Cr_{2.0}$SiBeta after adsorption of pyridine at room temperature and after that desorption by outgassing 1 h under vacuum of 10^{-3} Pa at 150 °C. The several IR bands at 1637, 1622, 1610, 1546, 1490, and 1450 cm^{-1} are observed for AlBeta related to Bronsted acidic centres (the bands at 1637 and 1546 cm^{-1}), Lewis acidic centres (the bands at 1622, 1610 and 1450 cm^{-1}), Brønsted and Lewis acidic centres (the band at 1490 cm^{-1}). The bands typical of pyridinium cations are seen at 1545 and 1637 cm^{-1}, indicating the presence of Brønsted acidic centres related to the acidic proton of Al—O(H) —Si groups, in line with earlier data [45]. The bans at 1450 cm^{-1} correspond to pyridine interacting with strong Lewis acidic centres (Al^{3+}). The band at 1490 cm^{-1} corresponds to pyridine interacting with both Brønsted and Lewis acidic centres.

The ^{27}Al MAS NMR of AlBeta zeolite posses 4 resonances (Fig. 4). The signals at 54.8 and 52.5 ppm associated to aluminum atoms present in two types of the tetrahedral environment of the framework. The signals at −1.7 and −10 ppm correspond to aluminum atoms in two types of octahedral environment. The first narrow peak, could be attributed to aluminum atoms in a tetrahedral environment near water molecules and the second a large peak could be attributed to extraframework species. Due to dealumination, the ^{27}Al NMR spectrum of SiBeta zeolite (Fig. 4) present only one a small signal at −52.5 ppm corresponding to aluminum atoms in the framework of zeolite [46,47].

The ^{29}Si MAS NMR spectrum of AlBeta (Fig. 5) shows two peaks at –114.5 and −111.0 ppm related to two crystallographic sites of the framework, Si atom in a $Si(OSi)_4$ (Q^4) environment. The signals at −102.2 and −106.1 ppm correspond to two Q^3 species, $(OSi)_3Si(OH)$ and $(OSi)_3Si(Al)$ groups, respectively. ^{29}Si MAS NMR spectrum of SiBeta (Fig. 5) is very similar to that of AlBeta. Only the signal at −106.1 ppm disappeared as a result of dealumination [48].

The ^{1}H MAS NMR of the AlBeta zeolite (Fig. 6) shows a broad signal at 4.7 ppm due to bridging hydroxyl protons (Si(OH)Al). The small signal at 1.37 corresponds to proton of SiOH groups. In the ^{1}H MAS NMR spectrum of SiBeta (Fig. 6) two main signals at 4.5 and 1.37 ppm, related to the protons of hydrogen bonded Si—OH groups present at vacant T-atom sites and to the protons of isolated Si—OH groups respectively [49,50]. Two peaks at 7 and 3.22 ppm are attributed to protons of water molecules and of hydrogen bonded Si—OH groups located in a second type of crystallographic site [51].

Moreover, dealumination leads also to significant reduction of basic sites number. The CO_2-TPD profiles for both materials are reported on Fig. 2B. In the case of AlBeta one intensive and a broad maximum ca. 200 °C with high temperature shoulder appeared, confirming presence of weak and medium basic sites which can be assigned to desorption weakly adsorbed CO_2 (physisorbed) and decomposition of carbonates like species. In contrast, the amount of CO_2 adsorbed on dealuminated support (SiBeta) is much lower than that on parent AlBeta support. Two maxima with very low intensity at about 200 and 350 °C appear. The quantitative calculation reported in Table 1 indicates that the total amount of CO_2 adsorbed on SiBeta is more than 8 times lower than on AlBeta.

3.2. Catalysts characterization

Using SiBeta support the series of Cr-containing SiBeta catalysts was prepared by wet impregnation. Based on AlBeta support the $Cr_{2.0}$AlBeta reference catalyst was prepared as well. Base characterization results of SiBeta series are summarized in Table 2.

Chemical analysis confirms good reproducibility of Cr incorporation in to the Beta zeolite. Both BET and Langmuir specific surface areas as well as total pore volume drops gradually with the total Cr content indicating that chromium deposition on SiBeta leads to porosity and surface area reduction, simultaneously.

The decrease of the 2θ value of the narrow main diffraction line around 2θ of 22.60° after introduction of Cr ions (Fig. 1) indicates some expansion of the Beta structure and suggests that the latter are incorporated into lattice sites. The 2θ value of this diffraction line decreases from 22.71 (SiBeta) to 22.64 ($Cr_{0.5}$SiBeta), 22.61 ($Cr_{1.0}$SiBeta) and 22.56° ($Cr_{2.0}$SiBeta) which indicates expansion of the matrix after incorporation of chromium ions into framework of SiBeta support. For higher Cr content, the decreasing of the 2θ value of this diffraction line is not observed (Fig. 1), so it suggests that for higher amount than 2 Cr wt % the Cr ions are introduced in the extra-framework position of the zeolite structure.

In contrast, the same 2 theta value of the main diffraction line at 22.55 for AlBeta and $Cr_{2.0}$AlBeta suggests that upon wet impregnation of AlBeta support with $Cr(NO_3)_3$ precursor expansion of zeolite matrix do not occurred. It indicates that Cr ions are introduced in the extra-framework position of Beta structure.

The incorporation of Cr leading to $Cr_{0.5}$SiBeta, $Cr_{1.0}$SiBeta and $Cr_{2.0}$SiBeta induces a reduction of intensity of the bands of silanol groups, isolated and hydrogen bonded at 3735 and 3524 cm^{-1} respectively (Fig. 3). Similar change has been observed for incorporation of vanadium and cobalt ions into SiBeta suggesting that silanol groups are

consumed in the reaction with chromium nitrate and Cr ions are simultaneously incorporated into framework of Beta zeolite, in agreement with later reports [41,44]. In addition, introduction of Cr ions in the AlBeta support leads to decreasing of Brønsted acid sites from 235.6 μmol g^{-1} for AlBeta to 227.3 μmol g^{-1} $Cr_{2.0}$AlBeta and Lewis acid sites from 134.8 μmol g^{-1} for AlBeta to 126.4 μmol g^{-1} for $Cr_{2.0}$AlBeta. For SiBeta and $Cr_{2.0}$SiBeta only traces of Brønsted and Lewis acid sites are observed.

The incorporation of chromium in SiBeta and AlBeta causes a decrease in the signal corresponding to the $(OSi)_3Si(OH)$ group (−102.2 ppm), which suggests an interaction between the chromium and the silanols of the zeolite (Fig. 5). The effect is much more important on $Cr_{2.0}$SiBeta than on $Cr_{2.0}$AlBeta.

In presence of chromium, the signals of bridging hydroxyl protons in AlBeta (4.7 ppm) and the signal of H-bonded Si—OH groups present at vacant T-atom sites in SiBeta (4.5 ppm) are very disturbed (Fig. 6). These modifications are due to the paramagnetic properties of chromium, which indicates a proximity between the species.

Furthermore, an oxidation state of chromium species in fresh samples was monitored using UV–vis diffuse reflectance spectroscopy (UV–vis DRS). Fig. 7A summarizes the spectra recorded in the range of 225–800 nm that is characteristic for charge transfer (CT) and d-d transition of chromium species. In all cases, in the CT transition region two peaks at 270 nm and 360 nm are detected. These peaks are assigned to CT of Cr^{6+}-O^{2-} transition in monochromate species attached with support [52,53]. In the case of catalysts with 5 or higher wt % of Cr an additional bands with low intensity in d-d region appeared (Fig. 7A). These two bands are characteristic for spin-allowed d-d transitions of Cr^{3+} [52–55]. Moreover, the band at 600 nm is asymmetric and has two low energy shoulders ca. 650 nm and 705 nm, which are assigned to spin-forbidden transition of Cr(III) (inset to Fig. 7A) [43]. The UV–vis DRS results indicate that below 5 wt % of Cr_{total} on SiBeta surface predominate Cr(VI) species while at and above this content Cr(VI) and Cr(III) species coexists.

Presence of Cr(VI) species in fresh samples is confirmed by H_2-TPR experiments (Fig. 7B). In all cases a single reduction maximum between 450 to 470 °C was observed. This maximum is assigned to reduction of Cr(VI) to Cr(III) species [54–56]. However, over ordered and unordered silica supports a deeper reduction of Cr(VI) to Cr(II) may also occur [27,28,56–58].

Quantitative results of H_2-TPR (Table 2) reveal that the hydrogen consumption rises with the Cr_{total} content indicating systematic rises of redox Cr(VI) species concentration. However, the ratio of H_2/Cr_{total} drops from 1.46 to 0.81 as Cr content rise from 0.5 to 7 wt % suggesting that with Cr_{total} content rises faster contribution of non redox Cr species (mainly Cr_2O_3 amorphous and crystalline) than redox ones. UV–vis DRS results (Fig. 6A) confirm that above 2 wt % rise the intensity of the d-d transition bands characteristic of Cr(III) species which are non-redox in nature while XRD indicates α-Cr_2O_3 formation above 5 wt % of Cr (Fig. 1).

3.3. Catalytic performance

Initially, the catalytic performances of all materials was investigated in CO_2-PDH process at 550 °C. Table 3 summarized initial specific activity, propane and carbon dioxide conversion as well as propene yield and selectivity to hydrocarbon products. The catalytic results for reference $Cr_{2.0}$AlBeta catalyst and several others Cr-based materials reported in literature are summarized as well.

It is clear from Table 3 that Cr_xSiBeta exhibits high catalytic performance, similar to other well know chromium oxide-based system supported on mesoporous silica supports (SBA-1, SBA-15, MCM-41, MSU-x) or active carbon. In Cr_xSiBeta series maximum initial yield 27.2 % was obtained on the sample with 7 wt % of Cr.

Moreover, it is clear that dealumination significantly improve both activity and selectivity. In the case of $Cr_{2.0}$AlBeta reference catalyst, the low selectivity to propylene is due to high concentration of strong acid sites over AlBeta support which prefer cracking of propane. Thus, over $Cr_{2.0}$AlBeta in product predominates methane, ethane and ethene produced in cracking reaction.

The variation of propane conversion and selectivity to propene vs. time-on-stream (TOS) are summarized in Fig. 8. Over all materials investigated conversion of propane drops with TOS, slightly for Cr-containing SiBeta zeolite with low Cr content ($Cr_{0.5}$SiBeta and $Cr_{1.0}$SiBeta) and much significantly for Cr-containing SiBeta zeolite with higher Cr content (higher than 2 Cr wt %). The selectivity to propene variation has opposite trend than propane conversion. It is also clear that in all cases the deactivation has not monotonic trend. It is faster at the beginning of the process and slow down with TOS.

To clarify deactivation process the catalysts was investigated upon catalytic test by UV–vis DRS. During the CO_2-PDH process over $Cr_{2.0}$SiBeta and $Cr_{2.0}$AlBeta the spectra were collected in two time period. The first period between 0–1 min and second ones between 1–240 min on stream. The Fig. 9 summaries the spectra collected in these two periods.

In both cases, spectra of degassed in helium samples (fresh catalysts before CO_2-PDH process) have two main maxima at 270 nm and 360 nm characteristic for CT transitions of Cr(VI) species. These maxima are reduced rapidly during first minute in contact with CO_2-C_3H_8 mixture (Fig. 9A and C). Simultaneously, new broad bands between 650–700 nm appear indicating reduction of Cr(VI) to Cr(III)/Cr(II) species. The letter species were found to be catalytically active in non-oxidative dehydrogenation of hydrocarbons [56]. Their also involve in the dehydrogenation with CO_2 [10,27,28]. Ohisih et al. [59] have proposed redox cycle between Cr(II) and Cr(III) species in which CO_2 acts as a mild oxidant. However, CO_2 is very weak oxidant. As we found previously Cr(VI) species reduced with CO selectively to Cr(II) species are very slowly re-oxidized by ultrapure CO_2 (additionally deoxygenated and dry) [62]. This may suggest that in the case of chromium-containing SiBeta catalyst an oxidation role of CO_2 cannot be responsible alone for observed promoting effect.

In the second time period (between 1–240 min on stream) continuous rise of the intensity in whole range was observed that confirms a darkening of the sample due to coke formation. Tracking of the intensity variation at 1000 nm indicates that darkening of the catalysts is faster at the beginning of the process and slow down with TOS unlike to propylene yield (inset to Fig. 9B and D). This variation of coke formation rate with TOS can be explained based on higher reactivity of propylene than propane. Because coke is produced more easily from propene its high yield leads to faster deactivation. Similar effect was observed in propane dehydrogenation over CrO_x/Al_2O_3 [63,64].

Fig. 10 shows variation between initial propene yield (after 10 min on stream) and hydrogen consumption (from H_2-TPR) that is proportional to number of redox Cr species for several various supported chromium oxide based catalysts including also Cr_xSiBeta.

Over different Cr-containing Beta materials the yield of propene rise with the number of redox Cr species which on various silicas depend on their pore structure and specific surface area of method of Cr incorporation/deposition as well as total Cr content. Typically, the yield rises with the increase of total Cr content up to the maximum value (monolayer coverage). After exceeding the monolayer coverage of support the redox Cr species are no longer stabilized (attached directly with support) and during the preparation there are decompose to less active and non-redox Cr_2O_3 particles. In Cr_xSiBeta series linear proportion between formation rate and number of redox species is observed up to 2 wt % of Cr. After exceeding this content catalytic performance did not correlate further with number of redox sites. In this respect the Cr_xSiBeta catalysts exhibits quite different behavior than chromium ox-

ide-based catalysts supported on ordered mesoporous silica (SBA-1 or SB-15). In the latter case propane rate was proportional to redox Cr species in wide range (between 07–13.6 wt % of Cr) while in Cr_xSiBeta series the yield of propene reminds constant at and above 5 wt % of Cr.

Finally, the effect of CO_2 on catalytic performance was investigated. Fig. 11 shows the variation of formation rate of propene, carbon monoxide and hydrogen with TOS in the dehydrogenation of propane in the presence and absence of CO_2, respectively. The switching process was carried out over $Cr_{2.0}$SiBeta and $Cr_{2.0}$AlBeta catalysts.

Promoting effect of CO_2 on formation rate of propene was observed over $Cr_{2.0}$SiBeta catalyst. In each cycle with CO_2 addition, the formation rate of propene was higher than in the cycles without it. Similar promoting effect was observed over chromium oxide-based catalysts supported on different pure siliceous supports, such as non-ordered SiO_2 or ordered MCM-41, SBA-15, SBA-1, MSU-x [5,9–11,14,15,27,28]. Typically, CO_2 addition enhances propene formation in comparison with PDH carried out using dilution with inert gas only [5,27,28]. Over $Cr_{2.0}$SiBeta, in CO_2 presence, rises formation rate of propene and carbon monoxide while at the same time decreases formation rate of hydrogen. It should be pointed hear that addition CO_2 never stops formation of hydrogen. Changes of formation rate of propene and hydrogen in cycles with and without CO_2 are similar suggesting that positive effect of CO_2 on propene production is due mainly due to shifting propane dehydrogenation equilibria via RWGS reaction. A good catalytic performance of Cr-containing catalysts in RWGS reaction was confirmed previously [13,27]. The equilibria calculations for two-step pathway of CO_2-PDH process i.e. for PDH reaction coupling with RWGS reaction and for single PDH confirm that CO_2 addition enhances significantly equilibrium conversion of propane [66]. Under reaction conditions applied in this work (p = 1 atm, t = 550 °C and feed with molar ratio C_3H_8:CO_2:Inert = 1:5:9 or C_3H_8:Inert = 1:14) the equilibrium conversion of propane rise from 70 % in PDH process to 89 % in CO_2-PDH process [2].

Taking in count above and considering very weak oxidative abilities of CO_2 against reduced Cr species it can be conclude that over chromium-containing SiBeta catalysts propene is produced mainly by PDH pathways facilitated by hydrogen removing in RWGS. Propane oxidative dehydrogenation (PODH) pathway has small contribution because CO_2 reoxidize very slowly reduced Cr species. Scheme 1 summarized both possible pathways responsible for CO_2 promoting effect on formation rate of propene.

It should be pointed hear that the promoting effect observed in the case of $Cr_{2.0}$SiBeta is similar to those observed on Cr-based catalysts supported on ordered or unordered mesoporous silicas. Over all these catalysts CO_2 addition enhance only partially propene formation (10–25 %). Comparing to others catalytic systems, for instance palladium supported on Ce-based supports the promoting the effect of CO_2 on Cr-based systems is moderate [3]. This variation of CO_2 effect with catalyst can be explained by different contribution of PODH and PDH pathways. In the case of Pd/Ce-based catalysts a dissociation of CO_2 to active O species and CO over ceria-based support facilitated both PODH and RWGS reactions, while over Cr/Silica based (or Si reach supports) catalysts such dissociation is not pronounced thus propene is produced mainly in PDH reaction.

In the contrast, over $Cr_{2.0}$AlBeta reference catalyst CO_2 exerts negative effect, e.g. the formation rate of propene drops in the process carried out with CO_2. In this respect the $Cr_{2.0}$AlBeta exhibits similar catalytic behavior to CrO_x/γ-Al_2O_3 catalyst [2,5,11]. In the latter case the poisoning effect of CO_2 was assigned to strong CO_2 adsorption on the surface of γ-Al_2O_3. FTIR investigation with CO_2 as a probe molecule have revealed that on the surface of CrO_x/γ-Al_2O_3 carbon dioxide is strongly adsorbed in form of carbonates which may limit dehydrogenation of propane [2]. The quantitative CO_2-TPD measurements show that amount CO_2 adsorption on AlBeta is much higher than over dealuminated form (SiBeta) (Table 1). This confirms stronger interaction of CO_2 with AlBeta which may explain poisoning effect observed over the $Cr_{2.0}$AlBeta zeolite catalyst.

4. Conclusions

Catalytic performance of chromium-containing SiBeta catalysts was investigated in the dehydrogenation of propane to propene in CO_2 assistance. Dealumination with acid nitrate leads to significantly reduction of Si/Al module from 17 to 1000. This has great impact on catalytic performance in CO_2-PDH process. A comparative catalytic results indicate that the promoting effect of CO_2 propylene formation was observed on $Cr_{2.0}$SiBeta. On this dealuminated form of Beta zeolite both the yield and selectivity to propene rise in the presence of CO_2. In contrasts, on $Cr_{2.0}$AlBeta zeolite catalyst CO_2 exerts negative effect similar to poisoning effect observed over γ-Al_2O_3 based chromium oxide catalyst. Moreover, in series of Cr_xSiBeta catalysts a correlation between number of redox Cr species and catalytic performance was found.

Declaration of Competing Interest

None.

References

[1] https://www.economic-plant.com/component/tags/tag/polypropylene.html, (Accessed 14 June 2019).
[2] P. Michorczyk, K. Zeńczak, R. Niekurzak, J. Ogonowski, Pol. J. Chem. Technol. 14 (2012) 77–82.
[3] E. Nowicka, C. Reece, S.M. Althahban, K.M.H. Mohammed, S.A. Kondrat, D.J. Morgan, Q. He, D.J. Willock, S. Golunski, C.J. Kiely, G.J. Hutchings, ACS Catal. 8 (2018) 3454–3468.
[4] E. Gomez, S. Kattel, B. Yan, S. Yao, P. Liu, J.G. Chen, Nat. Commun. 9 (2018) 1398.
[5] I. Takahara, W. Chang, N. Mimura, M. Saito, Catal. Today 45 (1998) 55–59.
[6] X. Zhang, Y. Yue, Z. Gao, Catal. Lett. 83 (2002) 19–25.
[7] K. Nakagawa, C. Kajita, N. Ikenaga, M. Nishitani-Gamo, T. Ando, T. Suzuki, Catal. Today 84 (2003) 149–157.
[8] M. Botavina, G. Martra, Y. Agafonov, N. Gaidai, N. Nekrasov, D. Trushin, S. Coluccia, A. Lapidus, Appl. Catal. A: Gen. 347 (2008) 126–132.
[9] H. Li, Y. Yue, C. Miao, Z. Xie, W. Hua, Z. Gao, Catal. Commun. 8 (2007) 1317–1322.
[10] K. Takehira, Y. Ohishi, T. Shishido, T. Kawabata, K. Takaki, Q. Zhang, Y. Wang, J. Catal. 224 (2004) 404–416.
[11] M. Kocoń, P. Michorczyk, J. Ogonowski, Catal. Lett. 101 (2005) 53–57.
[12] Y. Wang, Y. Ohishi, T. Shishido, Q. Hang, K. Takehira, Stud. Surf. Sci. Catal. 146 (2003) 725–728.
[13] P. Michorczyk, J. Ogonowski, React. Kinet. Catal. Lett. 87 (2005) 177–183.
[14] P. Michorczyk, J. Ogonowski, P. Kuśtrowski, L. Chmielarz, Appl. Catal. A: Gen. 349 (2008) 62–69.
[15] L. Liu, H. Li, Y. Zhang, Catal. Commun. 8 (2007) 565–570.
[16] Y. Wang, Y. Ohishi, T. Shishido, Q. Zhang, W. Yang, Q. Guo, H. Wan, K. Tkehira, J. Catal. 220 (2003) 347–357.
[17] H. Xiao, J. Zhang, P. Wang, X. Wang, F. Pang, Z. Zhang, Y. Tan, Catal. Sci. Technol. 6 (2016) 5183–5195.
[18] P. Michorczyk, J. Ogonowski, Appl. Catal. A: Gen. 251 (2003) 425–433.
[19] B. Xu, B. Zheng, W. Hua, Y. Yue, Z. Gao, J. Catal. 239 (2006) 470–477.
[20] B. Zheng, W. Hua, Y. Yue, Z. Gao, J. Catal. 232 (2005) 143–151.
[21] F. Zhang, C. Miao, Y. Yue, W. Hua, Z. Gao, Chin. J. Chem. 30 (2012) 929–934.
[22] M. Chen, J. Xu, Y.M. Liu, Y. Cao, H.Y. He, J.H. Zhuang, K.N. Fan, Catal. Lett. 124 (2008) 369–375.
[23] M. Chen, J. Xu, F.Z. Su, Y.M. Liu, Y. Cao, H.Y. He, K.N. Fan, J. Catal. 256 (2008) 293–300.
[24] P. Michorczyk, P. Kuśtrowski, L. Chmielarz, J. Ogonowski, React. Kinet. Catal. Lett. 82 (2004) 121–130.
[25] X.-L. Xue, W.-Z. Lang, X. Yan, Y.-J. Guo, ACS Appl. Mater. Interfaces 9 (2017) 15408–15423.
[26] I. Takahara, M. Saito, M. Inaba, K. Murata, Catal. Lett. 102 (2005) 201–205.
[27] P. Michorczyk, P. Pietrzyk, J. Ogonowski, Microporous Mesoporous Mater. 161 (2012) 56–66.
[28] P. Michorczyk, J. Ogonowski, K. Zenczak, J. Mol. Catal. A: Chem. 349 (2011) 1–12.
[29] S. Wang, K. Murata, T. Hayakawa, S. Hamakawa, K. Suzuki, Appl. Catal. A: Gen. 196 (2000) 1–8.
[30] X. Ge, M. Zhu, J. Shen, React. Kinet. Catal. Lett. 77 (2002) 103–108.
[31] N. Mimura, I. Takahara, M. Inaba, M. Okamoto, K. Murata, Catal. Commun. 3 (2002) 257–262.

[32] P. Kuśtrowski, P. Michorczyk, L. Chmielarz, Z. Piwowarska, B. Dudek, J. Ogonowski, R. Dziembaj, Termochim. Acta 471 (2008) 26–32.
[33] J.B. Higgins, R.B. LaPierre, J.L. Schlenker, A.C. Rohrman, J.D. Wood, G.T. Kerr, W.J. Rohrbaugh, Zeolites 8 (1988) 446–452.
[34] S.-B. Liu, J.-F. Wu, L.-J. Ma, T.-C. Tsai, I. Wang, J. Catal. 132 (1991) 432–439.
[35] Y. Zhang, Y. Li, J. Gu, S. Tian, P. Ning, Korean J. Chem. Eng. 35 (2018) 1932–1940.
[36] M.A. Camblor, A. Corma, J. Perez-Pariente, Zeolites 13 (1993) 82–87.
[37] E.P. Reddy, L. Davydov, G. Smirniotis, Panagiotis, J. Phys. Chem. B 106 (2002) 3394–3401.
[38] A. Rokicińska, M. Drozdek, B. Dudek, B. Gil, P. Michorczyk, D. Brouri, S. Dzwigaj, P. Kuśtrowski, Appl. Catal. B: Environ. 212 (2017) 59–67.
[39] K.A. Chalupka, W.K. Jozwiak, J. Rynkowski, W. Maniukiewicz, S. Casale, S. Dzwigaj, Appl. Catal. B 146 (2014) 227–236.
[40] S. Dzwigaj, P. Massiani, A. Davidson, M. Che, J. Mol. Catal. A 155 (2000) 169.
[41] S. Dzwigaj, M.J. Peltre, P. Massiani, A. Davidson, M. Che, J. Chem. Soc. Chem. Commun. 87 (1998).
[42] S. Dzwigaj, M. Matsuoka, R. Franck, M. Anpo, M. Che, J. Phys. Chem. B 102 (1998) 6309.
[43] S. Dzwigaj, M. Che, J. Phys. Chem. B 110 (2006) 12490.
[44] S. Dzwigaj, M. Matsuoka, R. Franck, M. Anpo, M. Che, J. Phys. Chem. B 110 (2006) 12490.
[45] S. Dzwigaj, P. Massiani, A. Davidson, M. Che, J. Mol. Catal. A: Chem. 155 (2000) 169–182.
[46] R. Baran, Y. Millot, T. Onfroy, J.-M. Krafft, S. Dzwigaj, Microporous Mesoporous Mater. 163 (2012) 122–130.
[47] R. Hajjar, Y. Millot, P.P. Man, M. Che, S. Dzwigaj, J. Phys. Chem. C 112 (2008) 20167–20175.
[48] S. Dzwigaj, Y. Millot, C. Méthivier, Michel Che, Microporous Mesoporous Mater. 130 (2010) 162–166.
[49] G.L. Woolery, L.B. Alemany, R.M. Dessau, A.W. Chester, Zeolites 6 (1986) 14–16.
[50] L.W. Beck, J.F. Haw, J.L. White, J. Am. Chem. Soc. 116 (1994) 9657–9661.
[51] P.I. Kyriienko, O.V. Larina, N.O. Popovych, S.O. Soloviev, Y. Millot, S. Dzwigaj, J. Mol. Catal. A: Chem. 424 (2016) 27–36.
[52] B.M. Weckhuysen, I.E. Wachs, R.A. Schoonheydt, Chem. Rev. 96 (1996) 3327–3350.
[53] M. Lezanska, G.S. Szymanski, P. Pietrzyk, Z. Sojka, J.A. Lercher, J. Phys. Chem. C 111 (2007) 1830–1839.
[54] A.G. Gaspar, L.C. Dieguez, J. Catal. 220 (2003) 309–316.
[55] A.G. Gaspar, J.L.F. Brito, L.C. Dieguez, J. Mol. Catal. A: Chem. 203 (2003) 251–266.
[56] A. Hakuli, M. Harlin, L. Backman, O. Krause, J. Catal. 184 (1999) 349–356.
[57] M. Gierada, P. Michorczyk, F. Tielens, J. Handzlik, J. Catal. 340 (2016) 122–135.
[58] C.S. Kim, S.I. Woo, J. Mol. Catal. 73 (1992) 249–263.
[59] Y. Ohishi, T. Kawabata, T. Shishido, K. Takaki, Q. Zhang, Y. Wang, K. Takehira, J. Mol. Catal. A: Chem. 230 (2005) 49–58.
[60] J.F.S. de Oliveira, D.P. Volanti, J.M.C. Bueno, A.P. Ferreira, Appl. Catal. A: Gen. 558 (2018) 55–66.
[61] F. Zhang, R. Wu, Y. Yue, W. Yang, S. Gu, C. Miao, W. Hua, Z. Gao, Microporous Mesoporous Mater. 145 (2011) 194–199.
[62] P. Michorczyk, J. Ogonowski, Chem. Commun. 48 (2012) 7283–7285.
[63] R.L. Puurunen, B.G. Beheydt, B.M. Weckhuysen, J. Catal. 204 (2001) 253–257.
[64] R.L. Puurunen, B.M. Weckhuysen, J. Catal. 210 (2002) 418–430.
[65] P. Michorczyk, J. Ogonowski, M. Niemczyk, Appl. Catal. A: Gen. 374 (2010) 142–149.
[66] M.A. Atanga, F. Rezaei, A. Jawad, M. Fitch, A.A. Rownaghi, Appl. Catal. B: Environ. 220 (2018) 429–445.